

Study on the oxygen isotope effect in A-site ordered manganite $RBaMn_2O_6$ ($R = \text{La, Pr, Nd, Sm}$)

G. Y. Wang, K. H. Wong and Y. Wang*

*Department of Applied Physics and Materials Research Center,
the Hong Kong Polytechnic University,
Hong Kong SAR, China*

(Dated: November 22, 2018)

A-site ordered manganites $RBaMn_2O_6$ ($R = \text{La, Pr, Nd, Sm}$) were synthesized and the oxygen isotope effect in them was studied. It was found that the substitution of ^{16}O by ^{18}O has caused increases in both the Neel temperature (T_N) and the charge ordering temperature (T_{CO}) and an decrease in the Curie temperature (T_C). The isotope exponent is small on T_C and T_{CO} compared with that in A-site disordered manganites such as $\text{La}_{1-x}\text{Ca}_x\text{MnO}_3$, which may be caused by weaker electron-phonon coupling in A-site ordered ones. But the isotope exponent of T_N is large for $R = \text{La}$. We didn't observe the large oxygen-isotope shift that occurs in $\text{NdBaMn}_2\text{O}_6$, where a multicritical point is believed to appear near $R = \text{Nd}$, and strong fluctuation due to the competition between ferromagnetic metal and charge ordering phase should be present.

PACS numbers: 71.38.-k, 75.30.-m

I. INTRODUCTION

Perovskite-related manganites, e.g. $R_{1-x}A_x\text{MnO}_3$ ($R = \text{Y}$ and rare earth metals, $A = \text{Ca}$ and Sr), have been studied extensively since the colossal magnetoresistance (CMR) phenomenon was first observed in $\text{La}_{0.66}\text{Ca}_{0.33}\text{MnO}_3$ ¹. Complex phase diagram has been observed in them, where ferromagnetic metal (FM), antiferromagnetic (AF) insulator, charge ordering (CO) state, and orbital ordering (OO) state present under different conditions. The evolution of magnetic and electronic properties in manganites have been investigated by changing parameters including temperature, magnetic field, pressure, hole doping level, size of A-site atom, doping on B-site, the quenched disorder, mismatch effect, and so on.² It is now widely accepted that the CMR effect is based on the phase competition between FM state and insulating state in nanometer length scale, and will be much enhanced near a bicritical point. A small bandwidth can also enhance the CMR effect, and quenched disorder will expand the parameter space where this effect can be observed³.

It is known that the radii of the cations are a critical factor to determine the crystal structure and properties of the perovskite manganites. For example, calcium and strontium ions, with the radii $r_{\text{Ca}^{2+}} = 1.34 \text{ \AA}$ and $r_{\text{Sr}^{2+}} = 1.44 \text{ \AA}$, respectively, can readily substitute La^{3+} ($r = 1.36 \text{ \AA}$) because of their radii are similar. However, Ba ($r = 1.61 \text{ \AA}$) has a rather low solubility in the system due to the much larger radius. Especially for half-doping level, a novel structure $RBaMn_2O_6$ with ordered A-site ions is obtained with special treatment

(depending on the difference of ion radii between R^{3+} and Ba^{2+}).^{4,5,6,7,8,9,10,11,12} In A-site ordered manganites, the R -O and Ba-O layers alternatively stack along the c -axis, doubling the lattice constant $c(2a_P$, where a_P is the axis of the simple perovskite cell). The A-site ordered manganites $RBaMn_2O_6$ exhibit different properties from the A-site disordered ones $R_{0.5}\text{Ba}_{0.5}\text{MnO}_3$, such as higher Curie temperature (T_C) and charge ordering temperature (T_{CO}), and the disappearance of spin glass (SG) state^{10,11,12}. They are divided into three different groups according to their properties: (1). $R = \text{Y}$ and Ho-Tb , a structure phase transition at T_t , a CE-type charge/orbital ordering (CO/OO) transition at T_{CO} , and an AF transition at T_N ; (2). $R = \text{Gd-Sm}$, a CE-type CO/OO transition at T_{CO1} , an AF transition at T_N , and another CO/OO transition at T_{CO2} with stack pattern different from the former one; and (3). $R = \text{Nd-La}$, a ferromagnetic transition at T_C and an AF transition at T_N . A multicritical point is also observed near $R = \text{Nd}$, where three ordered states, i.e., FM, A-type AF, and CO/OO states, compete with each other¹¹. However, the attempt to find CMR effect in this region is in vain, and large magnetoresistance can only be found when quenched disorder is introduced back into this system¹³.

Oxygen isotope exchange is an useful tool to study the electron-phonon coupling in materials, because it can avoid the change in chemical environment and physical structure due to other doping type, and introduce only small change in oxygen mass and hence the energy of phonon.^{14,15} Giant oxygen isotope effect has been found in CMR materials such as $\text{La}_{0.8}\text{Ca}_{0.2}\text{MnO}_3$ (21 K shift in T_C), indicating the presence of small polarons in it¹⁵. In this paper, we have studied the oxygen isotope effect in A-site ordered manganites $RBaMn_2O_6$ ($R = \text{La, Pr, Nd, Sm}$), aiming to establish a physical picture of the electron-phonon coupling in them and the relationship between quenched disorder and CMR effect. It was found

*Corresponding author; Electronic address:
apywang@inet.polyu.edu.hk

that the oxygen isotope effect on T_C and T_{CO} is small, which may be caused by the absence of A-site disorder. But the oxygen isotope effect on T_N of $\text{LaBaMn}_2\text{O}_6$ is large, which should be attributed to the fragileness of the AF transition in this composition.

II. EXPERIMENT DETAILS

Ceramic samples of A-site ordered RBaMn_2O_6 ($R = \text{La, Pr, Nd, and Sm}$) were prepared by solid-state reaction method with stoichiometric $R_2\text{O}_3$ (except for $R = \text{Pr}$ with Pr_6O_{11}), BaCO_3 , and MnO_2 , which has been reported everywhere^{9,10}. But for the following oxygen isotope exchange, a process different from previous one¹⁴ was employed, due to the sensitivity of A-site ordering to the heat treatment and oxygen pressure. A ceramic sample was cut into two pieces, and sealed into two quartz tubes (one with $^{18}\text{O}_2$ and another with $^{16}\text{O}_2$) of a tube furnace. The samples were first heated to 900 °C for 48 h to ensure the oxygen isotope exchange. It should be noticed that the A-site order maybe partly destroyed after this heat treatment, as reported in literature^{8,12}. After the samples were cooled to room temperature, the oxygen gas was pumped out and some hydrogen gas was filled into the tubes. Then the samples were heated to 950 °C for 5 hours, to reduce the sample and reconstruct the A-site ordered structure. After the treatment the system was cooled to 350 °C, then the tubes were evacuated again in order to remove the residual hydrogen and water (formed during the high temperature treatment). Subsequently oxygen gas was filled into the two tubes, one with $^{18}\text{O}_2$ and another with $^{16}\text{O}_2$. The samples were kept at 350 °C for 24 h to oxidize RBaMn_2O_5 to RBaMn_2O_6 . The oxygen isotope enrichment is determined by the weight change of samples. The ^{18}O samples have about 80(± 5)% ^{18}O and 20(± 5)% ^{16}O . The magnetization of samples were measured by vibrating sample magnetometer (Lakeshore 7400) from 80K to 400K. The resistivity were measured in cryostat with a helium compressor by four probe method. To reduce the measurement error, all the data were recorded during the warming process. To confirm the oxygen isotope enrichment, Raman spectra were recorded at room temperature by a Horiba HR800 micro-Raman system, with a 488 nm laser as the excitation source.

III. RESULT AND DISCUSSION

X-ray diffraction was performed on ^{16}O and ^{18}O samples of RBaMn_2O_6 ($R = \text{La, Pr, Nd, and Sm}$) to check the phase purity and the presence of A-site ordering. No impurity phase was discernible in the x-ray diffraction profiles. The signature of A-site ordering, i.e. the (001) peak with $c \sim 2a_P$, was observed in both kinds of samples (data not shown here), which confirmed the effectiveness of hydrogen annealing on the reconstruction of A-site or-

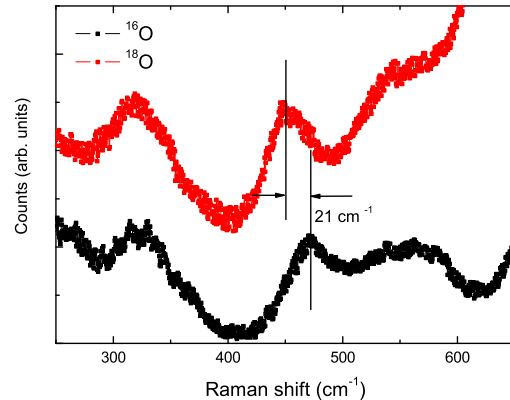


FIG. 1: (Color online) Raman spectra at room temperature for the ^{16}O and ^{18}O samples of $\text{LaBaMn}_2\text{O}_6$, respectively. The shift of Raman peak has been marked by two vertical lines, from which the 76% oxygen isotope enrichment can be deduced.

dering. The Raman spectra of samples were also recorded for the calculation of oxygen isotope enrichment. Fig. 1 shows the Raman spectra for the ^{16}O and ^{18}O samples of $\text{LaBaMn}_2\text{O}_6$. A peak located at 471 cm^{-1} was shifted to 450 cm^{-1} after the oxygen isotope substitution. The frequency of Raman mode f is reciprocally proportion to the square root of oxygen mass: $f(^{18}\text{O})/f(^{16}\text{O}) = \sqrt{16/M'}$. The oxygen isotope enrichment deduced from Raman shift is 76%, consistent with that deduced from the mass increase (80 \pm 5%).

The temperature dependence of magnetization (normalized to the data at 400K) for the ^{16}O and ^{18}O samples of RBaMn_2O_6 ($R = \text{La, Pr, and Nd}$) are shown in Fig. 2. All the data were recorded during the warming cycle for field cooling (FC) under a field of 100 Oe and zero field cooling (ZFC) situations. Ferromagnetic order is observed in all three samples. After the substitution of ^{16}O by ^{18}O , T_C is shifted to a lower temperature, marked by two horizontal arrows in Fig. 2. The shifts of T_C are -2.2 K, -4.6 K, and -3.8 K for $R = \text{La, Pr, and Nd}$, respectively. Comparing with the T_C shift in A-site disordered samples, for instance, $\Delta T_C = 21$ K for $\text{La}_{0.8}\text{Ca}_{0.2}\text{MnO}_3$ ¹⁵, and even a metal-insulator transition caused by oxygen isotope exchange,¹⁶ the current ones are much smaller. With decreasing temperature, a decrease in FC magnetization can be found in all the three ^{16}O samples, which is attributed to the CE-type antiferromagnetic transition for $R = \text{La}$, and A-type antiferromagnetic transition for $R = \text{Pr}$ and Nd ⁸. Here, we regard T_N as the temperature at which the maximum of magnetization in FC curves is achieved, as indicated by the perpendicular arrows in Fig. 2. For the ^{18}O samples, T_N is shifted to a higher temperature, and the shifts are 20 K, 4 K, and 2 K for $R = \text{La, Pr}$ and Nd , respectively.

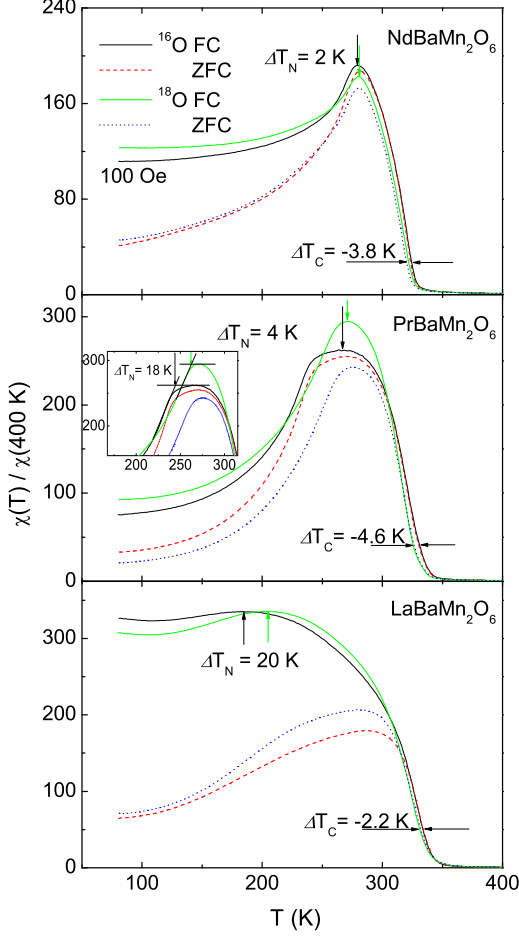


FIG. 2: (Color online) Temperature dependence of magnetization for the ^{16}O and ^{18}O samples of $R\text{BaMn}_2\text{O}_6$ ($R = \text{La}, \text{Pr}, \text{and Nd}$) at $H = 100$ Oe. The shift of T_C and T_N has been marked by horizontal arrows and vertical arrows, respectively. Inset shows another way to define the shift of T_N , which give a larger value.

It should be pointed out that the T_N shift is strongly affected by the way how it was defined. For example, we will get 18 K for $R = \text{Pr}$, if we determine the T_N shift as the inset of Fig. 2. The shift of T_N is distinct for $R = \text{La}$, but almost smeared out completely for $R = \text{Nd}$. This is very strange, since the critical region is believed to located near $R = \text{Nd}$, where fluctuation should be enhanced due to the competition of three ordered FM, A-type AFM and CO/OO states.

Fig. 3 shows the temperature dependence of magnetization (normalized to 400K) and resistivity (normalized to 380K) of $\text{SmBaMn}_2\text{O}_6$. It should be noted that the magnetic field used here is 1000 Oe. The shape of the magnetization is a little different from that reported in literature^{4,8,11}, which may be caused by slight fluctuation in sample composition among different groups. For

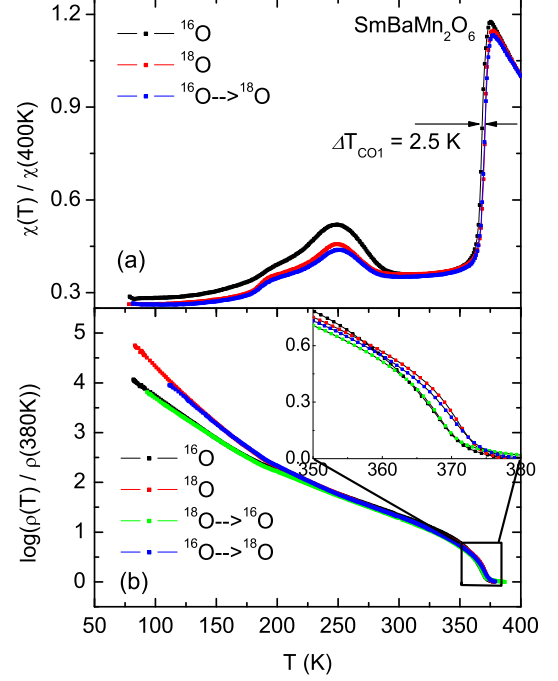


FIG. 3: (Color online) Temperature dependence of (a) magnetization (normalized to 400 K) and (b) resistivity (normalized to 380 K) for the ^{16}O and ^{18}O samples of $\text{SmBaMn}_2\text{O}_6$. Some data from back-exchanged samples are also presented. Inset of (b) shows the enlarged figure near the area of the first CO/OO transition.

the ^{16}O sample, the sharp decrease in the magnetization at 374 K (T_{CO1}) is related to the first charge/orbital ordering transition⁴, associated with an abrupt increasing of resistivity. When ^{16}O is replaced by ^{18}O , this ordered temperature is shifted to a higher temperature with $\Delta T_{\text{CO1}} = 2.5\text{K}$, consistent with that in resistivity shown in the inset of Fig. 3(b). At 248 K, a peak is observed in the magnetization curve, which is attributed to the CE-type AF transition⁴. This transition, however, is not reflected in the resistivity curve. The oxygen-isotope shift of T_N can only be seen in magnetization, from 248K to 250K. It should be emphasized that the magnetization in the ^{18}O sample is smaller than that in the ^{16}O sample. At about 193K, the second CO/OO transition occurs, which shows a slight kink in magnetization and a change of slope in resistivity. And the kink in magnetization is clearer in the ^{18}O sample. But the shift of T_{CO2} is difficult to calculate due to either the faintness of this kink in the ^{16}O sample, or the smallness of the oxygen-isotope shift. Powder neutron diffraction has given the evidence that the magnetic period in c -axis at $T < T_{\text{CO2}}$ is $4a_P$, and deduced ABAB-type stacking pattern of Mn-O layer along this direction⁴. However, recent resonant soft x-ray powder diffraction showed that the stacking

is AAAA-type along c -axis¹⁷. From the Goodenough-Kanamori rules, ABAB stacking pattern will produce ferromagnetic coupling while AAAA stacking pattern will produce AF coupling among the Mn-O layers in the c direction. The sudden drop in magnetization at T_{CO2} , caused by the oxygen isotope substitution, may be regarded as an evidence for the AAAA-type stacking.

The oxygen isotope exponents for A-site ordered manganites $RBaMn_2O_6$ ($R = \text{La, Pr, Nd, and Sm}$) are shown in Fig. 4 (a), which are calculated using the formula: $\alpha = -d\ln T/d\ln M = (16 \times (T_{16} - T_{18})) / (T_{16} \times (17.52 - 16))$. The oxygen isotope effects on the transition temperature are presented in Fig. 4 (b), vs the radii of R^{3+} . Generally, the substitution of ^{16}O by ^{18}O will soften the phonon, and increase the effective mass of electrons by some degree of electron-phonon coupling. Then the bandwidth of bare electron will be reduced, which strengthens the insulating phase and weakens the metal phase. This is the reason that the CO/OO ordering temperature T_{CO1} , associated with a metal-insulator transition in resistivity, is shifted to a higher temperature for $R = \text{Sm}$. The increased resistivity at low temperature in the ^{18}O sample is also an evidence for the reduced bandwidth. It is believed that T_C is proportional to the effective bandwidth of electrons¹⁸, so the substitution of ^{16}O by ^{18}O will decrease the T_C , as we have observed for $R = \text{La, Pr and Nd}$. On the other hand, decreasing bandwidth means reduced hopping integral t , which will favor the AF interaction and suppress the ferromagnetic interaction between Mn ions. So the T_N is shifted to a higher temperature for $R = \text{La, Pr, Nd}$, in spite of the transition type A or CE⁸.

We then further consider the magnitudes of the oxygen-isotope shifts. First, all the shifts of T_C and T_{CO} are small compared with that in A-site disordered ones. Quenched disorder will reduce the bandwidth¹⁹ (this is the reason that the curie temperature in ordered $\text{LaBaMn}_2\text{O}_6$ is 50 K higher than that in disordered $\text{La}_{0.5}\text{Ba}_{0.5}\text{MnO}_3$), which enhanced the relative importance of electron-phonon coupling², or in other word, the oxygen isotope shift of T_C . For $R = \text{Sm}$, the absence of disorder will also make the CO phase tough, which suppress the relative importance of electron-phonon coupling, and give small oxygen isotope shift. So the small oxygen isotope shift of T_C and T_{CO} in ordered $RBaMn_2O_6$ is accessible. And the T_C shift for $R = \text{La}$ is the smallest, due to the highest T_C (or largest bandwidth) in it. In fact, small oxygen isotope effect not only observed in A-site ordered manganites here, but also observed in other A-site ordered perovskite materials such as $RBaCo_2O_{5+x}$ ²¹. One may expect larger oxygen-isotope shift on T_C in $\text{Nd}_{1-x}\text{Sm}_x\text{Mn}_2\text{O}_6$, since it seems that the $r_{R^{3+}}$ of the critical point should be slightly smaller than $r_{Nd^{3+}}$ in our experiment.

Second, the isotope shift of T_N is large for $R = \text{La}$, but small for $R = \text{Nd}$. Neutron powder diffraction experiment shows that the FM transition in $RBaMn_2O_6$ is a second-ordered one, while the AF transition is a first-

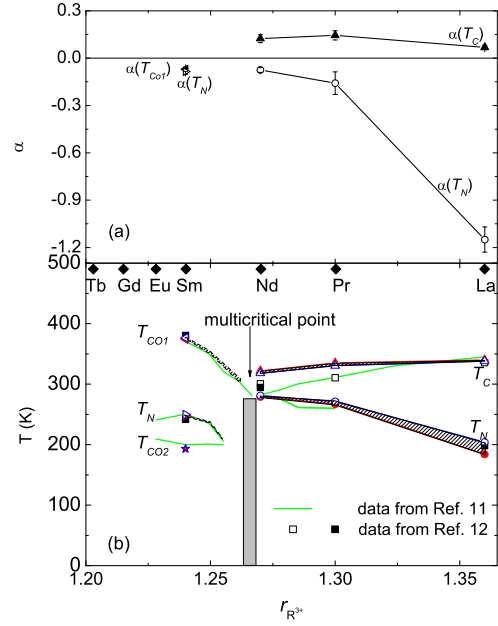


FIG. 4: (Color online) Part of the phase diagram for $RBaMn_2O_6$ ($R = \text{La, Pr, and Nd}$). Green line are the data taken from Ref. 11, square data are taken from Ref. 12. Red solid points and blue hollow points are for our ^{16}O and ^{18}O samples, respectively. Hatched areas indicate the possible change caused by oxygen isotope exchange.

ordered one^{8,22}. It is obvious that the lattice will couple more strongly to the first-ordered transition. This is the reason that we observed a large oxygen-isotope shift in T_N but not in T_C for $R = \text{La}$. The AF transition is especially fragile for $R = \text{La}$, and the nuclear magnetic resonant experiment demonstrated that AF phase occupies only about half the volume of the whole sample²³. The fragility of T_N will also enhance the relative importance of electron-phonon coupling on it, and induces the largest oxygen isotope shift in our experiment. But for $R = \text{Nd}$, the case is different. The multicritical point is believed to locate near $R = \text{Nd}$, where enhanced fluctuation should be present due to the competition among FM, CO/OO phase, and A-type AF phase. In A-site disordered samples such as $(R,\text{Ca})\text{MnO}_3$ and $(R,\text{Sr})\text{MnO}_3$, the critical point is always related to the enhanced fluctuation due to the competition between FM phase and CO insulating phase, and the CMR effect^{2,20}. A large oxygen-isotope shift on T_N is also expected for $R = \text{Nd}$. However, T_N in $\text{NdBaMn}_2\text{O}_6$ is almost the highest in the phase diagram of $RBaMn_2O_6$ ^{11,24}, indicating the relatively strong AF phase in it. The firmness of AF phase will certainly reduce the relative importance of oxygen isotope substitution, and show limited response on it.

IV. CONCLUSION

In summary, oxygen isotope effect on the FM, AF transition, and CO/OO transition is studied for $R\text{BaMn}_2\text{O}_6$ ($R = \text{La, Pr, and Nd}$). Small oxygen isotope shift is observed on T_{CO1} for $R = \text{Sm}$, due to the tough CO state caused by the absence of A-site disorder. The first-ordered nature of AF phase for $R = \text{La}$ produces much larger oxygen isotope shift on T_N than on the second-ordered FM transition temperature T_C . For $R = \text{Nd}$, the isotope effect on T_C is slightly enhanced due to the reduced band width comparing with that of $R = \text{La}$; but

the oxygen isotope shift on T_N is smaller due to the relative strong AF phase in it.

ACKNOWLEDGMENTS

This work was supported by the Hong Kong Polytechnic University Postdoctoral Scheme (G-YX0C). The support from the Center for Smart Materials is also acknowledged.

-
- ¹ S. Jin, T. H. Tiefel, M. McCormack, R. A. Fastnacht, R. Ramesh, and L. H. Chen, *Science* **264**, 413 (1994).
 - ² E. Dagotto, T. Hotta, and A. Moreo, *Phys. Rep.* **344**, 1 (2001), and the references therein.
 - ³ E. Dagotto and Y. Tokura, *MRS Bulletin* **33**, 1037 (2008).
 - ⁴ T. Arima, D. Akahoshi, K. Oikawa, T. Kamiyama, M. Uchida, Y. Matsui, and Y. Tokura, *Phys. Rev. B* **66**, 140408(R) (2002).
 - ⁵ Anthony J. Williams and J. Paul Attfield, *Phys. Rev. B* **66**, 220405(R) (2002); Anthony J. Williams and J. Paul Attfield, *Phys. Rev. B* **72**, 024436 (2005).
 - ⁶ S. V. Trukhanov, I. O. Tryanchuk, M. Hervieu, H. Szymczak, and K. Brner, *Phys. Rev. B* **66**, 184424 (2002).
 - ⁷ T. Nakajima, H. Kageyama, and Y. Ueda, *J. Phys. Chem. Solids* **63**, 913 (2002).
 - ⁸ T. Nakajima, H. Kageyama, H. Yoshizawa, K. Ohoyama, and Y. Ueda, *J. Phys. Soc. Jpn.* **72**, 3237 (2003).
 - ⁹ D. Akahoshi, Y. Okimoto, M. Kubota, R. Kumai, T. Arima, Y. Tomika, and Y. Tokura, *Phys. Rev. B* **70**, 064418 (2004).
 - ¹⁰ F. Millange, V. Caignaert, B. Domengs, B. Raveau, and E. Suard *Chem. Mater.* **10**, 1974 (1998).
 - ¹¹ D. Akahoshi, M. Uchida, Y. Tomioka, T. Arima, Y. Matsui, and Y. Tokura, *Phys. Rev. Lett.* **90**, 177203 (2003).
 - ¹² T. Nakajima, H. Yoshizawa, and Y. Ueda, *J. Phys. Soc. Jpn.* **73**, 2283 (2004).
 - ¹³ Y. Ueda and T. Nakajima, *Prog. Solid State Chem.* **35**, 397 (2007).
 - ¹⁴ G. Y. Wang, T. Wu, X. G. Luo, W. Wang, and X. H. Chen, *Phys. Rev. B* **73**, 052404 (2006); G. Y. Wang, X. H. Chen, T. Wu, G. Wu, X. G. Luo, and C. H. Wang, *Phys. Rev. B* **74**, 165113 (2006).
 - ¹⁵ G. M. Zhao, K. Conder, H. Keller, and K. A. Mller, *Nature (London)* **381**, 676 (1995).
 - ¹⁶ N. A. Babushikina, L. M. Belova, O. Yu. Gorbenko, A. R. Kaul, A. A. Bosak, V. I. Ozhojin, and K. I. Kugel, *Nature (London)* **391**, 159 (1998).
 - ¹⁷ M. Garca-Fernndez, U. Staub, Y. Bodenthin, S. M. Lawrence, A. M. Mulders, C. E. Buckley, S. Weyeneth, E. Pomjakushina, and K. Conder, *Phys. Rev. B* **77**, 060402(R) (2008).
 - ¹⁸ N. Furukawa, *J. Phys. Soc. Jpn.* **64**, 2754 (1995).
 - ¹⁹ Y. Motome, N. Furukawa, and N. Nagosa, *Phys. Rev. Lett.* **91**, 167204 (2003).
 - ²⁰ Cengiz Sen, Gonzalo Alvarez, and Elbio Dagotto, *Phys. Rev. Lett.* **98**, 127202 (2007).
 - ²¹ K. Conder, E. Pomjakushina, V. Pomjakushin, M. Stingaciu, S. Streule, and A. Podlesnyak, *J. Phys.: Condens. Matter* **17**, 5813 (2005); E. Pomjakushina, K. Conder, and V. Pomjakushin, *Phys. Rev. B* **73**, 113105 (2006).
 - ²² T. J. Sato, J. W. Lynn, and B. Dabrowski, *Phys. Rev. Lett.* **93**, 267204 (2004).
 - ²³ Y. Kawasaki, T. Minami, Y. Kishimoto, T. Ohno, K. Zenmyo, H. Kubo, T. Nakajima, and Y. Ueda, *Phys. Rev. Lett.* **96**, 037202 (2006).
 - ²⁴ Y. Ueda and T. Nakajima, *J. Phys.: Condens. Matter* **16**, S573 (2004).